Chinese Journal of Catalysis 34 (2013) 1216–1223 催化学报 2013年 第34卷 第6期 | www.chxb.cn

available at www.sciencedirect.com

ScienceDirect

journal homepage: www.elsevier.com/locate/chnjc

Article

A novel approach for the preparation of phase-tunable TiO_2 nanocomposite crystals with superior visible-light-driven photocatalytic activity

YU Fuhai [a,b], WANG Junhu [a,*], ZHAO Kunfeng [a,b], YIN Jie [a,b], JIN Changzi [a], LIU Xin [a]

[a] *Dalian Institute of Chemical Physics, Chinese Academy of Sciences, Dalian 116023, Liaoning, China*
[b] *University of Chinese Academy of Sciences, Beijing 100049, China*

ARTICLE INFO

Article history:
Received 8 January 2013
Accepted 15 March 2013
Published 20 June 2013

Keywords:
Chemical solution process
Titanium oxide
Nanocomposite crystal
Phase modulation
Visible light
Photocatalysis
Adsorption capacity

ABSTRACT

A series of novel TiO_2 nanocomposite crystals with superior visible-light-driven photocatalytic activity were successfully prepared using a soft chemical solution process involving direct reaction of aqueous H_2O_2 with a 2-ethoxyethanol solution of tetraisopropyl titanate before calcination of the resulting peroxo-titanium complexes at 500 °C for 4 h. The synthesized TiO_2 samples are composed of anatase and rutile phases, and the ratio of rutile could be continuously tuned from 0 to 96% by altering the 2-ethoxyethanol volume. There are clear red-shifts in the UV-Vis absorption spectra and apparent band gap narrowing for the synthesized TiO_2 in comparison with Evonik P-25. The synthesized TiO_2 samples are found to be much more efficient for methylene blue degradation under visible-light irradiation. The optimized sample (2-ethoxyethanol: 5 ml; rutile in bulk: 46%) exhibits 5-fold higher adsorption capacity and 3-fold higher photocatalytic activity than those of Evonik P-25 ($\lambda \geq 400$ nm). Characterizations including X-ray diffraction and Raman spectroscopy reveal that the surface of the optimized TiO_2 sample only contains a small quantity of rutile. It is concluded that the surface phase composition and distribution of the TiO_2 nanocomposite crystals are essential to their greatly enhanced photocatalytic activities and strong adsorption capacities. In addition, the concentration of defects existing in the synthesized TiO_2 is also regarded to account for these enhanced properties.

1. Introduction

Since the discovery of hydrogen production via water splitting over TiO_2 by Fujishima and Honda [1] almost 40 years ago, the photocatalytic properties of TiO_2 [2–6] and many other kinds of semiconductor oxides [7–9] have been widely studied. In addition to water splitting, great potential has been found for self-cleaning materials [10–12] and trace contaminant degradation and mineralization [13–15] in the environment. However, there are two main shortcomings that considerably restrict the wider application of TiO_2 photocatalysts. First, the band gap of TiO_2 is about 3.0 eV for rutile and 3.2 eV for anatase. As a consequence, TiO_2 can only absorb ultraviolet light, which only makes up a small part (namely 3%–5%) of the energy of solar light. Different approaches have been pursued to narrow the band gap and thereby increase visible-light absorption. The most common approach is to dope TiO_2 with other ions. Different kinds of transition metal cations such as Fe^{3+},

* Corresponding author. Tel: +86-411-84379159; Fax: +86-411-84685940; E-mail: wangjh@dicp.ac.cn
This work was supported by the Chinese Academy of Sciences for "100 Talents" Project, the National Natural Science Foundation of China (11079036), and the Natural Science Foundation of Liaoning Province (20092173).
DOI: 10.1016/S1872-2067(12)60574-9 | http://www.sciencedirect.com/science/journal/18722067 | Chin. J. Catal., Vol. 34, No. 6, June 2013

Sn^{4+}, and Ti^{3+} [16–19] are reported to be effective in increasing visible-light absorption. Doping of anions C, N, and S into TiO_2 [20–24] is also reported to be effective for band gap narrowing. Although doped TiO_2 can exhibit great increases in light absorption, there is no remarkable corresponding increase in photocatalytic activity because the doping ions can also act as recombination centers for the photo-induced electron-hole pairs [25].

The synthesis of nanocomposites is another important approach for improving the photocatalytic performance of TiO_2 [26,27] because the resulting so-called hetero-junctions will promote the separation of photo-induced electron-hole pairs. Exposure of high energy facets can also enhance the photocatalytic activity of TiO_2 [28,29]. Furthermore, great progress has recently been achieved in the synthesis of pure TiO_2 with greatly increased visible-light absorption ability and enhanced visible-light-driven photocatalytic activity. For example, Chen et al. [30] reported a new kind of black TiO_2 that exhibited relatively efficient water-splitting activity under visible-light irradiation. Tao et al. [31] reported a two-dimensional phase of TiO_2 with a remarkably narrowed band gap of 2.1 eV. Etacheri et al. [32] reported a visible-light-active, high-temperature stable, and dopant-free TiO_2 anatase photocatalyst that was formed by the modification of amorphous TiO_2 with H_2O_2. Despite progress in narrowing the band gap of TiO_2, low adsorption capacity is still a barrier to be solved. As is known, TiO_2 can only photocatalytically degrade contaminants that come into contact with or are only tens of nanometers away from its surface. Therefore, the improvement of its adsorption capacity is of great significance for its wider application. In most cases, TiO_2 is combined with other sorbing materials (such as hydroxyapatite, activated carbon, and graphene) [33–36] to form a nanocomposite. Although it seems that TiO_2 based nanocomposites reported so far can exhibit increased adsorption capacity, their photocatalytic activities need to be further improved. Reports of the synthesis of pure TiO_2 with both increased adsorption capacity and superior photocatalytic activity under visible-light irradiation are rare.

Herein, we report the preparation, structural characterization, and superior visible-light-driven photocatalytic performance of a series of novel TiO_2 nanocomposite crystals that were successfully synthesized through a soft chemical solution process, in which an aqueous H_2O_2 solution and a 2-ethoxyethanol solution of tetraisopropyl titanate were mixed together to form a gel-like peroxo-titanium complex. The obtained peroxo-titanium complexes were then calcined at 500 °C for 4 h. The prepared TiO_2 samples were composed of anatase and rutile, and the phase compositions could be continuously tuned in a wide range by adjusting the volume of 2-ethoxyethanol. The surface crystal phase composition and distribution of the TiO_2 nanocomposites, and their defect concentration, were considered to be essential to their greatly enhanced photocatalytic activities and adsorption capacities. This is the first report of the synthesis of pure TiO_2 with both greatly enhanced adsorption capacity and superior visible-light-driven photocatalytic activity.

2. Experimental

2.1. Preparation of the TiO_2 samples

The soft chemical solution process used in the current study to prepare the TiO_2 nanocomposite crystals is a modified method previously reported by our group for the preparation of fine antimonic acid nanoparticles [37,38]. In this modified method, a peroxo-titanium complex was produced as a precursor by adding an aqueous H_2O_2 solution to a 2-ethoxyethanol solution of tetraisopropyl titanate [39]. All reagents were used without further purification. A typical synthesis procedure for the optimized TiO_2 sample (2-ethoxyethanol: 5 ml; rutile in bulk: 46%) is described as follows. Tetraisopropyl titanate (Aladdin, 98%, 2ml) was dissolved in 5 ml 2-ethoxyethanol ($C_2H_5OCH_2CH_2OH$, Alfa Aesar, 99%) under magnetic stirring. Then, 30 ml aqueous H_2O_2 solution (Kemiou, 30 wt%) was added to the tetraisopropyl titanate solution to form a peroxo-titanium complex. The obtained colloid solution was heated in a water bath at 50 °C for 30 min to produce an orange gel. After drying the orange gel in an oven at 120 °C overnight, the xerogel thus obtained was calcined at 500 °C for 4 h in a muffle furnace. A series of different TiO_2 nanocomposite crystals were synthesized by tuning the volume of 2-ethoxyethanol. A control sample of TiO_2 was also prepared without the introduction of 2-ethoxyethanol. The TiO_2 samples prepared are hereafter marked as *n*-TiO_2, in which *n* denotes the volume of 2-ethoxyethanol. The P-25 sample used as a standard was purchased from Evonik.

2.2. Characterization

X-ray diffraction (XRD) patterns were collected on a PW3040/60 X'Pert PRO (PANalytical) diffractometer equipped with a Cu K_α radiation source (λ = 0.1542 nm). A continuous mode was used for collecting data in the 2θ range from 10° to 80° operating at 40 kV and 40 mA. The amount of rutile phase present in each sample was calculated using the Spurr equation [40], $F_R = 1/[1 + 0.8\, I_A(101)/I_R(110)]$, where F_R is the amount of rutile in the anatase-rutile composite, and I_A (101) and I_R (110) are the anatase and rutile main peak intensity, respectively. In addition, the crystallite size of the different samples was calculated using the Scherrer Equation $\Phi = K\lambda/\beta\cos\theta$, where Φ is the crystallite size, λ is the X-ray wavelength used, K is the shape factor, β is the full line width at the half-maximum height of the main intensity peak, and θ is the diffraction angle of the peak.

Nitrogen adsorption-desorption measurements were performed at –196 °C with a Micromeritics ASAP 2010 instrument. Prior to the measurements, the samples were degassed at 110 °C for 1 h and at 250 °C for 4 h. The specific surface areas (A_{BET}) were calculated using the BET equation. Transmission electron microscopy (TEM) images were obtained on a JEOL JEM-2000EX microscope operating at 120 kV. Samples for TEM were prepared by dispersing the sample powder in methanol followed by sonication for 30 min. UV Raman spectra (325 nm laser) and visible-light Raman spectra (532 nm laser) were

measured at room temperature with a Jobin LabRAM HR 800 spectrometer at a spectral resolution of 2 cm^{-1}. UV-Vis diffuse reflectance spectra were obtained on a Cintra (GBC) apparatus equipped with an integrated sphere attachment using $BaSO_4$ as the reference. The band gaps of the samples were estimated from the onset of the absorption edge. X-ray photoelectron spectra (XPS) were recorded on an ESCALAB 250 X-ray photoelectron spectrometer with monochromated Al K_α anode. All binding energies were calibrated using contaminated carbon as an internal standard (C 1*s* = 284.5 eV).

2.3. Adsorption and photocatalytic property measurements

The adsorption capacity of the prepared series of TiO_2 nanocomposite crystals and the visible-light-driven photocatalytic degradation of methylene blue dye were separately evaluated using similar methods to those reported previously [9]. In the current study, a MAX 303 Xe lamp purchased from Asahi Spectra was used as a light source. An infrared light cut-off filter and a 400 nm long-pass filter were fitted to the Xe lamp to cut off the infrared and ultraviolet light. The TiO_2 sample (50 mg) was magnetically suspended in aqueous methylene blue solution (0.001%, 50 ml) in a 100 ml glass beaker. After allowing adsorption equilibrium in darkness for 30 min, the suspension was irradiated with a visible-light intensity of 8.8 mW/cm^2 using the Xe lamp. Aliquots (2 ml) were withdrawn from the suspension after the dark test and during visible-light irradiation at 15-min intervals, and the optical absorption spectrum of the supernatant was measured using a Cintra (GBC) apparatus. The adsorption capacity and photocatalytic degradation activity of the TiO_2 samples were mainly determined by the decrease in the absorbance of aqueous methylene blue solution at a wavelength of about 664 nm. The photocatalytic rate constant for methylene blue degradation (k) was determined from the first order plot using the equation $\ln(A_{eq}/A) = kt$ [28], where A_{eq} is the absorbance of methylene blue solution after adsorption equilibrium, A is absorbance after the time (t), and k is the first order rate constant.

3. Results and discussion

3.1. Structural characterization

The powder XRD analysis as shown in Fig. 1(a) indicates that the *n*-TiO_2 samples were well crystallized and composed of anatase and rutile. There are great differences in the diffraction peak intensities of $I_A(110)$ for anatase at around 25.30° and $I_R(101)$ for rutile at around 27.43°, which is direct evidence for changes in their phase compositions. The enlargement of the two diffraction peaks of selected *n*-TiO_2 samples shown in Fig. 1(b) further indicates that there are differences in the lattice dimensions. Variation of lattice dimensions is usually explained on the basis of defect concentration [32,41]. This is reasonable and also confirmed by XPS analysis as described below. This means that the defect concentrations in the lattice can be tuned by adjusting the volume of 2-ethoxyethanol used in the modified chemical solution process.

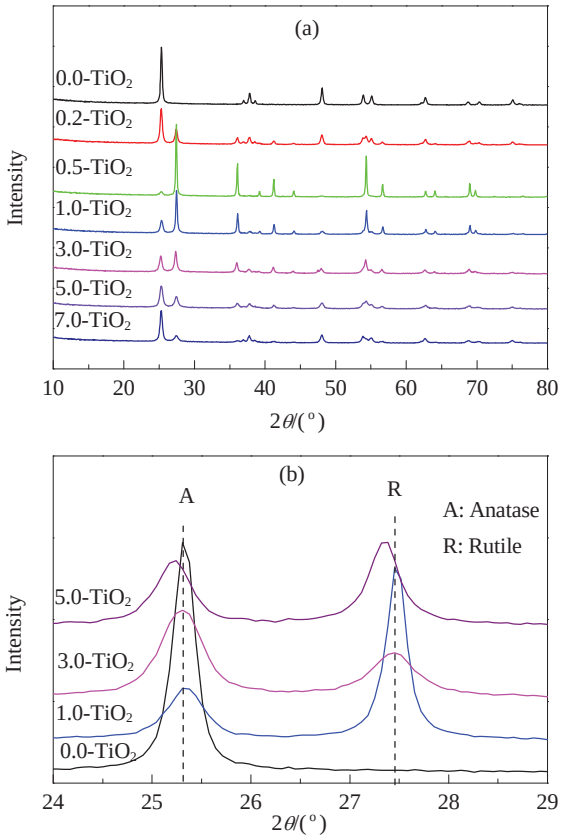

Fig. 1. XRD patterns (a) and an enlargement of the two diffraction peaks (b) of the *n*-TiO_2 samples (*n* = volume of 2-ethoxyethanol).

The phase composition and crystallite size values obtained from the Spurr and Scherrer equations are listed in Table 1. It was found that the TiO_2 (0.0-TiO_2) sample was completely anatase phase when no 2-ethoxyethanol was added to the synthesis solution. The content of rutile was at a maximum when 0.5 ml 2-ethoxyethanol was added. Further increases in the volume of 2-ethoxyethanol led to the decrease of rutile content. As a result, the content of rutile could be continuously tuned from 0 to 96%. As is known, the phase composition of TiO_2 can greatly influence its photocatalytic activity, and the preparation of mixed crystal phases is thought to be an effective approach for the improvement of the photocatalytic activity [42,43].

In addition to the phase composition, the crystallite size was also tunable. The crystallite size of the 0.0-TiO_2 sample was 43

Table 1
Phase compositions, crystallite size, band gap, and BET surface area of the *n*-TiO_2 samples.

Sample	Content of rutile (%)	Size (nm)		Band gap (eV)	A_{BET} (m^2/g)
		Anatase	Rutile		
P-25	20	20	45	3.1	41
0.0-TiO_2	0	43	—	2.9	68
0.2-TiO_2	36	24	20	2.9	51
0.5-TiO_2	96	—	20	2.8	77
1.0-TiO_2	80	26	29	2.9	51
3.0-TiO_2	58	24	28	2.9	45
5.0-TiO_2	46	21	25	2.9	55
7.0-TiO_2	29	25	18	2.9	35

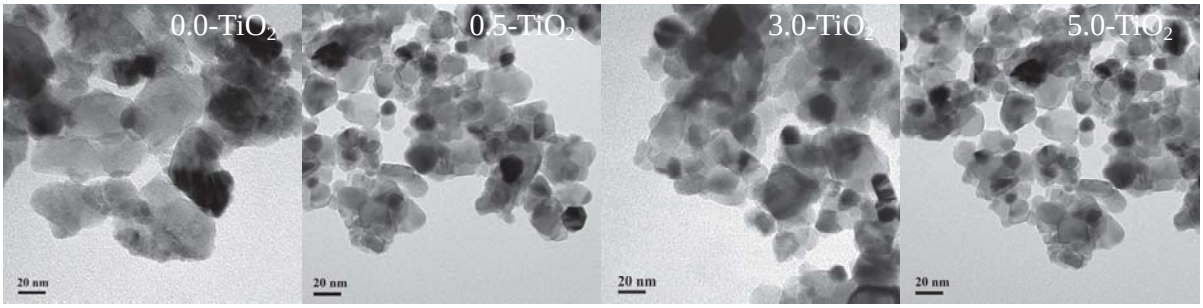

Fig. 2. TEM images of the *n*-TiO_2 samples.

nm. When 0.2 ml 2-ethoxyethanol was used, the crystallite size reduced to 24 nm for anatase and 20 nm for rutile. Therefore, the introduction of 2-ethoxyethanol can be used to effectively tune not only the phase composition but also the crystallite size. The TEM images of the *n*-TiO_2 samples shown in Fig. 2 further confirm that the addition of 2-ethoxyethanol can be used to tune the size of TiO_2 nanoparticles effectively. The particle size of the 0.0-TiO_2 sample is clearly larger than those of the others, which is in good agreement with the trend seen in the XRD results.

Table 1 also shows the BET surface areas of the *n*-TiO_2 samples, which varied from 35 to 77 m^2/g. The largest BET surface area was achieved when the volume of 2-ethoxyethanol was around 0.5 ml, which was about twice that of Evonik P-25. This sample also exhibited the smallest crystallite size as calculated by the Scherrer equation. However, there were no obvious differences between the specific surface areas of most of the *n*-TiO_2 samples prepared by the present modified chemical solution process. As is known, photocatalysis takes place on the surface of TiO_2. Therefore, a higher surface area usually leads to higher photocatalytic activity and adsorption capacity.

The phase compositions in the bulk region of the *n*-TiO_2 samples were determined by the XRD analysis. The more surface-sensitive Raman spectroscopic technique was further applied to identify the phase composition and distribution in the surface region of the *n*-TiO_2 samples [27]. As is shown in Fig. 3(a), strong bands at 395, 515, and 638 cm^{-1} are observable in the visible-light Raman spectrum of the 0.0-TiO_2 sample. All of these bands are ascribed to the anatase phase TiO_2, which is in good agreement with the XRD results. In the visible-light Raman spectrum of the 0.5-TiO_2 sample, strong bands of rutile phase at 235, 445, and 612 cm^{-1} are observable. However, there is still a weak band at 515 cm^{-1}, which indicates the co-existence of a small amount of anatase with a large amount of rutile in the 0.5-TiO_2 sample, which is also in good agreement with the XRD results.

It is reported that 532 nm laser light can probably penetrate into TiO_2 nanoparticles [27], in which case it will lead to almost the same information on the phase compositions and distribution of the *n*-TiO_2 samples in the surface and bulk regions being obtained from the Raman analysis. Taking this possibility into consideration, both 325 nm laser UV Raman spectra and 532 nm laser visible-light Raman spectra were measured for the 3.0-TiO_2 and 5.0-TiO_2 samples, to validate the results obtained for the surface region phase composition and distribution. As is shown in Fig. 3, the visible-light and UV Raman spectra of the 3.0-TiO_2 sample are very similar; both show that almost the same amount of anatase and rutile was contained in the 3.0-TiO_2 sample, comparable with the XRD results (see Table 1, 58% rutile for 3.0-TiO_2). In the visible-light and UV Raman spectra of the 5.0-TiO_2 sample, there is a slight difference in the intensity of 445 cm^{-1} band. However, both the visible-light and UV Raman results indicate that only a small quantity of rutile was distributed in the surface region (far from its bulk rutile content, 46%, see Table 1) of the 5.0-TiO_2 sample.

Combining the XRD and Raman spectroscopy results, it can be concluded that the surface composition and distribution are different from that in the bulk region for the 5.0-TiO_2 sample, while the surface composition and distribution are almost the same as that in the bulk region for the 0.0-TiO_2, 0.5-TiO_2, and 3.0-TiO_2 samples. Mixed phases of anatase and rutile coexisted

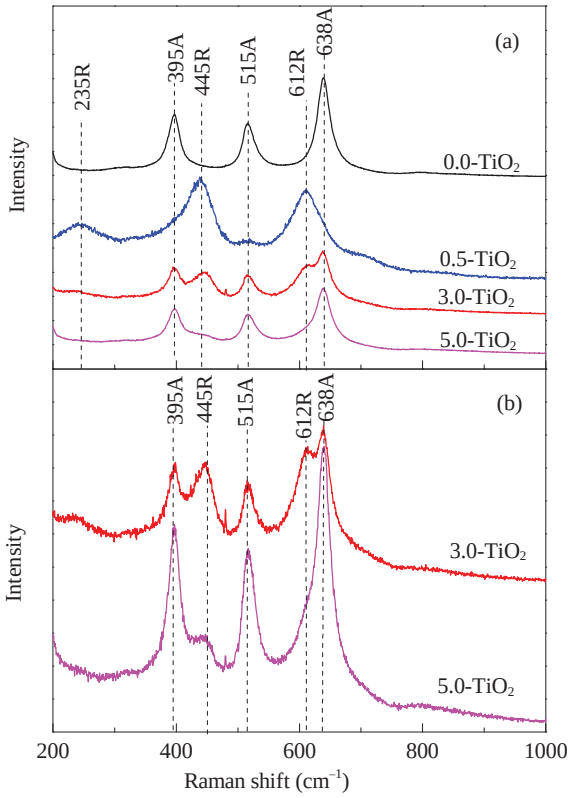

Fig. 3. Visible-light (a) and UV (b) Raman spectra of the *n*-TiO_2 samples for excitation laser lines of 532 nm and 325 nm, respectively.

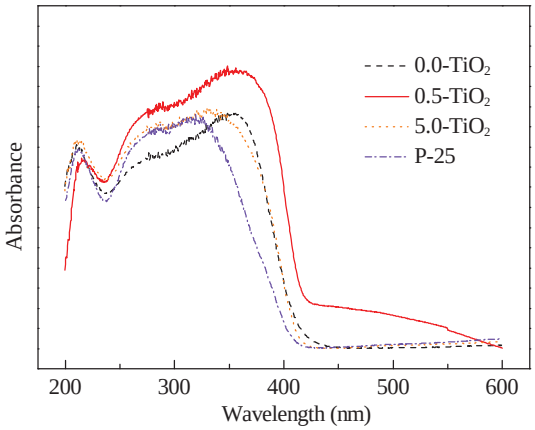

Fig. 4. UV-Vis diffuse reflectance spectra of Evonik P-25 and the *n*-TiO_2 samples.

in the 0.5-TiO_2, 3.0-TiO_2, and 5.0-TiO_2 samples, and the amount of rutile in the surface region should be in the order 0.5-TiO_2 >> 3.0-TiO_2 >> 5.0-TiO_2. The grain boundary between anatase and rutile likely promoted the separation of photo-generated electron-hole pairs, thus leading to the increase in their photocatalytic activity. It has been reported that the phase composition, distribution, defect existence, and concentration of a TiO_2 nanocomposite crystal are essential to their greatly enhanced photocatalytic activity and strong adsorption capacity [44–47].

3.2. Optical absorption properties

Figure 4 shows the UV-Vis diffuse reflectance spectra of selected *n*-TiO_2 samples and Evonik P-25. It can be seen that there are clear red-shifts in the spectra of the *n*-TiO_2 samples in comparison with that of P-25, which is direct evidence of band gap narrowing. Clear visible-light absorption at wavelengths over 400 nm was observed (420 nm for 0.0-TiO_2, 5.0-TiO_2, and 0.5-TiO_2). The band gaps were estimated to be 3.1 eV for P-25 and 2.9 eV for 0.0-TiO_2, 5.0-TiO_2, and 0.5-TiO_2, as listed in Table 1. As known, the commercial TiO_2 photocatalyst Evonik P-25 is also a mixture of anatase and rutile. However, the pure anatase (0.0-TiO_2) prepared by the present modified chemical solution process exhibited the increase of light absorption in comparison with that of P-25. Therefore, the increase of visible-light absorption due to the formation of rutile phase can be excluded. The pure anatase (0.0-TiO_2) and the two phase composites (5.0-TiO_2) share almost the same capacity in their optical absorption properties. This should mainly be due to the different phase composition and distribution of the 5.0-TiO_2 sample in the surface and bulk regions; only a small quantity of rutile was distributed in the surface region. The possible reason behind the increased visible-light absorption of the 0.0-TiO_2 and 5.0-TiO_2 samples is the existence and concentration of defects. As discussed above, the defect concentration should be related to the lattice dimension variations confirmed by the shifts of the diffraction peaks shown in Fig. 1(b). The largest red-shift was observed in the spectrum of the 0.5-TiO_2 sample. The other reason should be the 0.5-TiO_2 sample having the highest content of rutile (96%, see Table 1) because rutile has a relatively narrower band gap of 3.0 eV in comparison with that of anatase, 3.2 eV.

To obtain a better understanding of the increased visible-light absorption ability, XPS was used to characterize the chemical states of surface Ti and O in selected *n*-TiO_2 samples, as shown in Fig. 5. The XPS results exhibited decreased Ti $2p_{2/3}$ (Ti–O) binding energy for the *n*-TiO_2 samples prepared by the modified chemical solution process after the addition of 2-ethoxyethanol (Fig. 5(a)). The binding energy of pure anatase (0.0-TiO_2) was 458.5 eV. The anatase and rutile composites exhibited slightly decreased binding energy (458.2 eV for 0.5-TiO_2, 458.4 eV for 5.0-TiO_2) in comparison with that of the 0.0-TiO_2 sample. Similar decreases in O 1*s* binding energies were also identified for the *n*-TiO_2 samples (Fig. 5(b)). The values of Ti $2p_{2/3}$ (Ti–O) binding energy ranged from 458.2 to 458.5 eV, which are clearly lower than most of those reported for pure anatase, rutile, and mixed composite phases [48–50]. The lower Ti $2p_{2/3}$ (Ti–O) binding energy is direct evidence for the existence of oxide vacancies [51] in the *n*-TiO_2 samples, even for 0.0-TiO_2. The slightly decreased binding energy of 0.5-TiO_2 and 5.0-TiO_2 in comparison with that of 0.0-TiO_2 indicates a slight increase of oxide vacancy concentration in the *n*-TiO_2 samples prepared by the modified chemical solution process after the addition of 2-ethoxyethanol. The XPS results are consistent with those obtained from the XRD analyses. As described above, the XRD results indicated that crystal defects existed in the *n*-TiO_2 samples. It has been reported that the

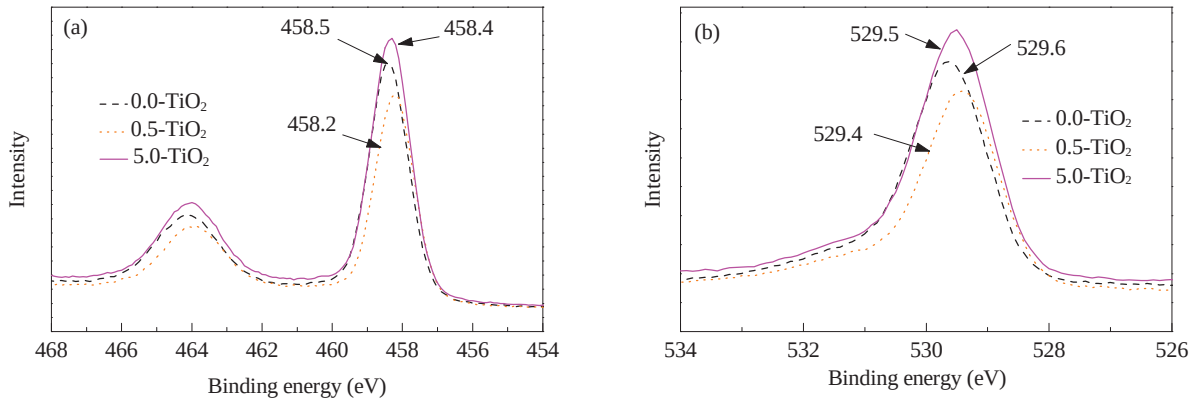

Fig. 5. Ti 2*p* (a) and O 1*s* (b) XPS spectra of the *n*-TiO_2 samples.

formation of oxide vacancies in the TiO_2 lattice can effectively promote the band gap narrowing, thus leading to a superior visible-light-driven photocatalytic activity [52–54]. So, excluding the influence of rutile phase, the increased visible-light absorption property of the *n*-TiO_2 samples should be mainly due to the formation of such oxide vacancies.

3.3. Adsorption and visible-light-driven photocatalytic properties

Figure 6 shows the adsorption and visible-light-driven methylene blue degradation photocatalytic activity of the *n*-TiO_2 samples. Figure 6(a) shows the removal percentage against adsorption and irradiation time, and Fig. 6(b) and (c) show the absorption spectra measured during methylene blue degradation over 0.0-TiO_2 and 5.0-TiO_2, respectively. It was found that all *n*-TiO_2 samples exhibited superior adsorption capacity for the methylene blue dye molecules in comparison with that of P-25. It was also found that the *n*-TiO_2 samples prepared with the addition of 2-ethoxyethanol exhibited photocatalytic activity superior to that of P-25 under visible-light irradiation. The photocatalytic activity of the 0.0-TiO_2 sample, which was completely anatase, was more or less the same as that of P-25. For the other *n*-TiO_2 samples, photocatalytic activity improved gradually with increasing 2-ethoxyethanol addition. The highest photocatalytic activity was achieved over the 5.0-TiO_2 sample (content of rutile in bulk: 46%). For the 0.5-TiO_2 sample (content of rutile: 96%), however, although its light absorption was significantly increased, its photocatalytic activity did not greatly increase owing to its phase composition. Kinetic studies were carried out to better compare the activities of the 0.0-TiO_2, 5.0-TiO_2, and P-25 samples, as shown in Fig. 7. The 5.0-TiO_2 sample was found to exhibit 3-fold and 4-fold higher visible-light-driven photocatalytic activity than that of P-25 and 0.0-TiO_2, respectively.

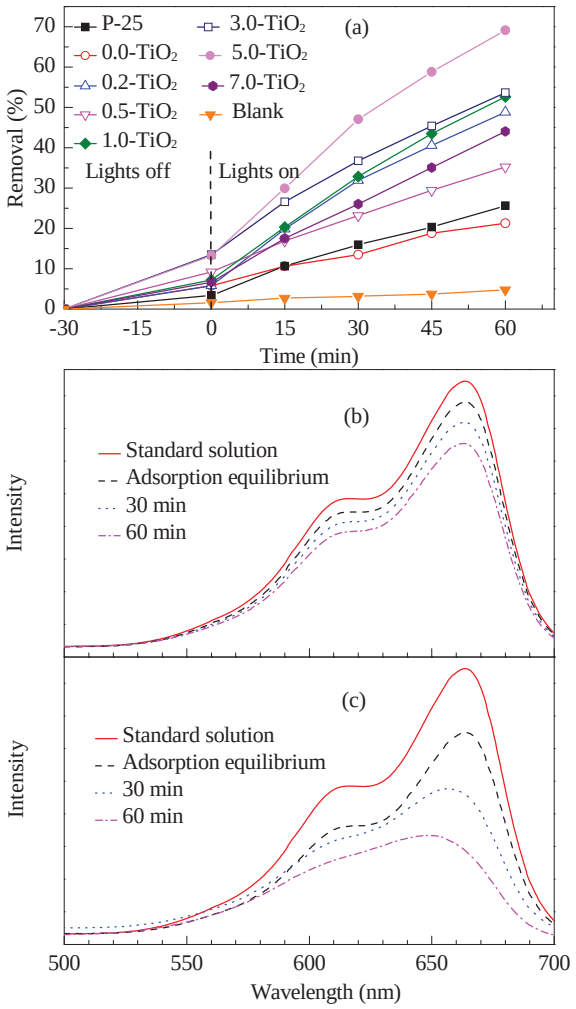

Fig. 6. Adsorption and visible-light-driven methylene blue degradation photocatalytic activity of the *n*-TiO_2 samples. (a) Removal percentage against adsorption and irradiation time; (b), (c) Absorption spectra of methylene blue degradation over 0.0-TiO_2 and 5.0-TiO_2, respectively. Reaction conditions: photocatalyst 1.0 mg/ml, methylene blue 0.001%, MAX 303 Xe lamp 8.8 mW/cm².

According to the XRD results, anatase and rutile type titania coexisted in the *n*-TiO_2 samples, and their mole ratios could be adjusted in a wide range by changing the volume of 2-ethoxythanol used in the modified chemical solution process. The introduction of 2-ethoxyethanol was also effective in tuning their crystallite sizes and even defect concentrations. Raman spectroscopic studies showed that the phase compositions and distribution of the 5.0-TiO_2 sample were clearly different in the surface and bulk regions, which implies that the surface phase composition and distribution were also effectively tuned by the introduction of 2-ethoxyethanol. The XPS results demonstrated that the increased visible-light absorption properties were mainly due to the formation of oxide vacancies in the *n*-TiO_2 crystal lattices. The concentrations of oxide vacancies in the 5.0-TiO_2 crystal lattices were likely larger than that of 0.0-TiO_2 and less than that of 0.5-TiO_2 because their Ti $2p_{2/3}$ (Ti–O) binding energies were in the order 458.5 eV (0.0-TiO_2) > 458.4 eV (5.0-TiO_2) > 458.2 eV (0.5-TiO_2). Taking structure, optical absorption, adsorption capacity, and visible-light-driven photocatalytic activity into consideration, it is concluded that besides an optimized crystal phase composition and distribution of the TiO_2 crystals in the surface region, an appropriate oxide vacancy concentration was also essential to the observed increased visible-light absorption, thus leading to band gap

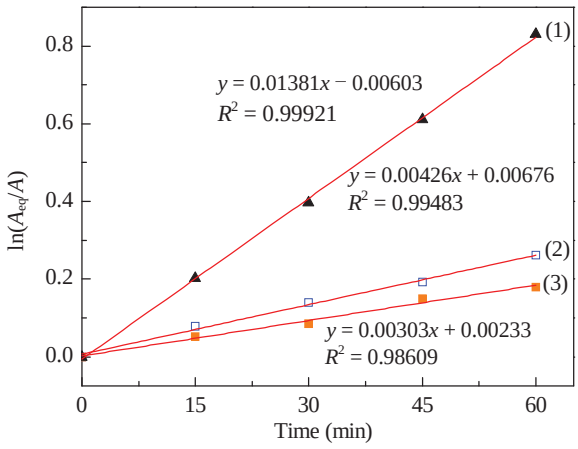

Fig. 7. Kinetic study of selected *n*-TiO_2 samples. (1) 5.0-TiO_2; (2) Degussa P-25; (3) 0.0-TiO_2.

narrowing, stronger adsorption capacity, and enhanced visible-light-driven photocatalytic activity.

In addition, the architecture of the anatase and rutile TiO_2 nanocomposite photocatalysts could be compared with a host(anatase)-guest(rutile) functional framework. The existence of grain boundaries is vital to the separation of photo-generated electrons and holes thus leading to enhanced photocatalytic activity [55,56]. Most importantly, the greatest enhanced photocatalytic properties are achieved when a very limited proper guest (rutile) is composited to the crystal lattice of the proper host (anatase) in the surface region. This should also be a key reason why the 5.0-TiO_2 sample exhibited the best photocatalytic performance among the *n*-TiO_2 samples although the co-existence of anatase and rutile in the surface region was also observed in the 0.5-TiO_2 and 3.0-TiO_2 samples. The role of host and guest could not be converted. The 0.5-TiO_2 and 5.0-TiO_2 samples had completely different anatase and rutile composited architecture, which resulted in a different promotion effect of their visible-light-driven photocatalytic activities. Further research will be needed to determine the fine-architectured structure of the *n*-TiO_2 samples in their surface regions.

4. Conclusions

A novel series of TiO_2 nanocomposite crystals with strong adsorption capacities and superior visible-light-driven photocatalytic activities were successfully synthesized through a modified chemical solution process by altering the amount of added 2-ethoxyethanol. Besides anatase/rutile mole ratio, crystallite size, and nanocomposite structure, an appropriate concentration of oxide vacancies formed in their lattice was also identified as the critical factor responsible for the strong adsorption capacity and superior visible-light-driven photocatalytic activity observed. The increased visible-light absorption properties and band gap narrowing were ascribed to the formation of oxide vacancies. The introduction of 2-ethoxyethanol resulted in a larger oxide vacancy concentration in comparison with the TiO_2 without 2-ethoxyethanol. The most optimized TiO_2 sample (2-ethoxyethanol: 5.0 ml; rutile in bulk 46%) had the desired oxide vacancy concentration and only a small quantity of rutile phase distributed in its surface region. The visible-light-driven photocatalytic activity of this sample was 3-fold and 4-fold higher than that of P-25 and TiO_2 prepared without 2-ethoxyethanol, respectively. This research provides a novel, convenient, and low-cost method for preparing pure TiO_2-based photocatalytic materials with strong adsorption capacity and superior visible-light-driven photocatalytic activity. These properties make it a promising material for wider application.

Acknowledgements

The authors would like to give special thanks to Dr. Long Hao and Prof. Junhua Dong (Institute of Metal Research, Chinese Academy of Sciences) for offering assistance to the XPS data collection.

References

[1] Fujishima A, Honda K. *Nature*, 1972, 238: 37
[2] Pal M, Serrano J G, Santiago P, Pal U. *J Phys Chem C*, 2007, 111: 96
[3] Peng C W, Ke T Y, Brohan L, Richard-Plouet M, Huang J C, Puzenat E, Chiu H T, Lee C Y. *Chem Mater*, 2008, 20: 2426
[4] Chuangchote S, Jitputti J, Sagawa T, Yoshikawa S. *ACS Appl Mater Inte*, 2009, 1: 1140
[5] Chen Y M, Zhong J, Chen F, Zhang J L. *Chin J Catal* (陈艳敏, 钟晶, 陈锋, 张金龙. 催化学报), 2010, 31: 120
[6] Wang L Y, Wang H X, Wang A J, Liu M. *Chin J Catal* (王丽燕, 王红霞, 王爱杰, 刘敏. 催化学报), 2009, 30: 939
[7] Mukherji A, Marschall R, Tanksale A, Sun Ch H, Smith S C, Lu G Q, Wang L Zh. *Adv Funct Mater*, 2011, 21: 126
[8] Mukherji A, Seger B, Lu G Q, Wang L Zh. *ACS Nano*, 2011, **5**: 3483
[9] Wang J, Nonami T. *J Mater Sci*, 2004, 39: 6367
[10] Bedford N M, Steckl A J. *Appl Mater Interf*, 2010, 2: 2448
[11] He D L, Meng X J, Tao Y C, Zhang L, Xiao F S. *Chin J Catal* (和东亮, 孟祥举, 陶艳春, 张琳, 肖丰收. 催化学报), 2009, 30: 83
[12] He J, Cai Q Z, Xiao F, Luo Q, Wang L J, Zhu D. *Chin J Catal* (何剑, 蔡启舟, 肖枫, 罗强, 王丽娟, 祝迪. 催化学报), 2009, 30: 1137
[13] Sopyan I, Watanabe M, Murasawa S, Hashimoto K, Fujishima A. *J Photochem Photobiol A*, 1996, 98: 79
[14] Zhu Y F, Shen W Z. *Appl Surf Sci*, 2010, 256: 7472
[15] Zhang J, Yan S, Fu L, Wang F, Yuan M Q, Luo G X, Xu Q, Wang X, Li C. *Chin J Catal* (张静, 阎松, 付鹿, 王飞, 原梦琼, 罗根祥, 徐倩, 王翔, 李灿. 催化学报), 2011, 32: 983
[16] Yu H G, Irie H, Shimodaira Y, Hosogi Y, Kuroda Y, Miyauchi M, Hashimoto K. *J Phys Chem C*, 2010, 114: 16481
[17] Wang X H, Li J G, Kamiyama H, Katada M, Ohashi N, Moriyoshi Y, Ishigaki T. *J Am Chem Soc*, 2005, 127: 10982
[18] Kaleji B K, Sarraf-Mamoory R, Nakata K, Fujishima A. *J Sol-Gel Sci Technol*, 2011, 60: 99
[19] Suriye K, Praserthdam P, Jongsomjit B. *Appl Surf Sci*, 2007, **253**: 3849
[20] Tryba B, Morawski A W, Inagaki M. *Appl Catal B*, 2003, 41: 427
[21] Asahi R, Morikawa T, Ohwaki T, Aoki K, Taga Y. *Science*, 2001, 293: 269
[22] Wang J, Tafen D N, Lewis J P, Hong Zh L, Manivannan A, Zhi M J, Li M, Wu N Q. *J Am Chem Soc*, 2009, 131: 12290
[23] Ohno T, Akiyoshi M, Umebayashi T, Asai K, Mitsui T, Matsumura M. *Appl Catal A*, 2004, 265: 115
[24] Liu E Q, Guo X L, Qin L, Shen G D, Wang X D. *Chin J Catal* (刘二强, 郭晓玲, 秦雷, 申国栋, 王向东. 催化学报), 2012, 33: 1665
[25] Choi W, Termin A, Hoffman M R. *J Phys Chem*, 1994, 98: 13669
[26] Choi S K, Kim S, Lim S K, Park H. *J Phys Chem C*, 2010, 114: 16475
[27] Zhang J, Xu Q, Feng Z C, Li M, Li C. *Angew Chem Int Ed*, 2008, 47: 1766
[28] Xiang Q J, Yu J G. *Chin J Catal* (向全军, 余家国. 催化学报), 2011, 32: 525
[29] Wu Q, Wu Z J, Li Y L, Gao H T, Pu L Y, Zhang T H, Du L X. *Chin J Catal* (吴谦, 吴志娇, 李永良, 高洪涛, 朴玲钰, 张天慧, 杜利霞. 催化学报), 2012, 33: 1743
[30] Chen X B, Liu L, Yu P Y, Mao S S. *Science*, 2011, 331: 746
[31] Tao J G, Luttrell T, Batzill M. *Nature Chem*, 2011, 3: 296
[32] Etacheri V, Seery M K, Hinder S J, Pillai S C. *Adv Funct Mater*, 2011, 21: 3744
[33] Nonami T, Hase H, Funakoshi K. *Catal Today*, 2004, 96: 113
[34] Li Y J, Li X D, Li J W, Yin J. *Water Res*, 2006, 40: 1119
[35] Williams G, Seger B, Kamat P V. *ACS Nano*, 2008, 2: 1487
[36] Li Y J, Chen W, Li L Y, Ma M Y. *Sci China Chem*, 2011, 54: 497

Graphical Abstract

Chin. J. Catal., 2013, 34: 1216–1223 doi: 10.1016/S1872-2067(12)60574-9

A novel approach for the preparation of phase-tunable TiO_2 nanocomposite crystals with superior visible-light-driven photocatalytic activity

YU Fuhai, WANG Junhu*, ZHAO Kunfeng, YIN Jie, JIN Changzi, LIU Xin
Dalian Institute of Chemical Physics, Chinese Academy of Sciences
University of Chinese Academy of Sciences

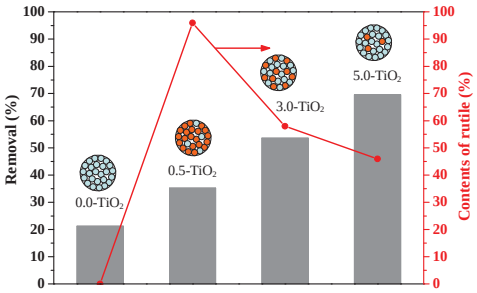

A novel approach for synthesis of phase-tunable TiO_2 is provided. The phase composition, distribution, and amount of oxygen vacancies are regarded as critical to the obtained superior visible-light-driven photocatalytic activity.

[37] Wang J, Ozawa K, Takahashi M, Takeda M, Nonami T. *Chem Mater*, 2006, 18: 2261
[38] Ozawa K, Wang J, Ye J H, Sakka Y, Amano M. *Chem Mater*, 2003, 15: 928
[39] Ichinose H, Terasaki M, Katsuki H. *J Sol-Gel Sci Technol*, 2001, 22: 33
[40] Spurr R A, Myers H. *Anal Chem*, 1957, 29: 760
[41] Yoon S D, Chen Y, Yang A, Goodrich T L, Zuo X, Arena D A, Ziemer K, Vittoria C, Harris V G. *J Phys: Condens Matter*, 2006, 16: 355
[42] Tseng Y H, Kuo C S, Huang C H, Li Y Y, Chou P W, Cheng C L, Wong M S. *Nanotechnology*, 2006, 17: 2490
[43] Hurum D C, Agrios A G, Gray K A, Rajh T, Thurnauer M C. *J Phys Chem B*, 2003, 107: 4545
[44] Dambournet D, Belharouak I, Amine K. *Chem Mater*, 2010, 22: 1173
[45] Testino A, Bellobono I R, Buscaglia V, Canevali C, D'Arienzo M, Polizzi S, Scotti R, Morazzoni F. *J Am Chem Soc*, 2007, 129: 3564
[46] Kawahara T, Konishi Y, Tada H, Tohge N, Nishii J, Ito S. *Angew Chem, Int Ed*, 2002, 41 :2811
[47] Bikondoa O, Pang C L, Ithnin R, Muryn C A, Onishi H, Thornton G. *Nat Mater*, 2006, 5: 189
[48] Herman G S, Gao Y. *Thin Solid Films*, 2001, 397: 157
[49] Sanjines R, Tang H, Berger H, Gozzo F, Margaritondo G, Levy F. *J Appl Phys*, 1994, 75: 2945
[50] Yamanaka S, Makita K. *J Porous Mater*, 1995, **1**: 29
[51] Rumaiz A K, Ali B, Ceylan A, Boggs M, Beebe T, Shah S I. *Solid State Commun*, 2007, 144: 334
[52] Ihara T, Miyoshi M. Ando M, Sugihara S, Iriyama Y. *J Mater Sci*, 2001, 36: 4201
[53] Osorio-Vargas P A, Pulgarin C, Sienkiewicz A, Pizzio L R, Blanco M N, Torres-Palma R A, Pétrier C, Rengifo-Herrera J A. *Ultrason Sonochem*, 2012, 19: 383
[54] Chen C H, Shieh J, Hsieh S M, Kuo C L, Liao H Y. *Acta Mater*, 2012, 60: 6429
[55] Yu J G, Xiong J F, Cheng B, Liu Sh W. *Appl Catal B*, 2005, 60: 211
[56] Yu J G, Wang B. *Appl Catal B*, 2010, 94: 295

晶相组成可调的高活性可见光应答型二氧化钛纳米复合光催化材料的制备

于福海[a,b], 王军虎[a,*], 赵昆峰[a,b], 尹 杰[a,b], 金长子[a], 刘 忻[a]
[a]中国科学院大连化学物理研究所, 辽宁大连116023
[b]中国科学院大学, 北京100049

摘要: 采用新的化学溶液法, 通过不同体积的钛酸四异丙酯的2-乙二醇单乙醚溶液与一定浓度的H_2O_2水溶液直接反应并对生成的钛过氧化配合物进行焙烧, 制备了一系列TiO_2光催化剂. 表征发现, 所得TiO_2样品为金红石和锐钛矿的纳米复合晶体, 改变2-乙二醇单乙醚的体积可实现金红石相比例在0~96%广范围的调变.与商业二氧化钛P-25相比, 所得的TiO_2紫外-可见光吸收谱出现明显红移, 间隙能降低, 在可见光照射下, 该样品对亚甲基蓝有良好的降解活性. 当2-乙二醇单乙醚的添加量为5 ml时, 所得样品体相中金红石相比例接近50%, 其光催化活性和吸附性能最好, 可分别是P-25的3倍和5倍. 拉曼光谱结合X射线衍射等表征结果表明, 该样品的表面仅含少量的金红石相. TiO_2纳米复合晶表面晶相的组成和分布对其光催化降解亚甲基蓝的活性及其吸附能力有直接的影响. 另外, TiO_2纳米复合晶的缺陷浓度也是增强其光吸收能力, 提高其可见光光催化活性的原因之一.

关键词: 化学溶液法; 二氧化钛晶体; 纳米复合物; 可见光; 光催化; 晶相调变; 吸附性能

收稿日期: 2013-01-08. 接受日期: 2013-03-15. 出版日期: 2013-06-20.
*通讯联系人. 电话: (0411)84379159; 传真: (0411)84685940; 电子信箱: wangjh@dicp.ac.cn
基金来源: 中国科学院"百人计划"; 国家自然科学基金(11079036); 辽宁省自然科学基金(20092173).
本文的英文电子版由Elsevier出版社在ScienceDirect上出版(http://www.sciencedirect.com/science/journal/18722067)